Solute segregation in directional solidification : Scaling analysis of the solute boundary layer coupled with transient hydrodynamic simulations

Marc Chatelain, Mickael Albaric, David Pelletier, Valéry Botton

Solute segregation in directional solidification: Scaling analysis of the solute boundary layer coupled with transient hydrodynamic simulations.

M.Chatelain[a], M. Albaric[a], D. Pelletier[a], V.Botton[b]
[a] *CEA/LITEN/DTS, INES, 50 avenue du Lac Léman, 73377 Le Bourget-du-Lac, France*
[b] *Laboratoire de Mécanique des Fluides et d'Acoustique, CNRS/Université de Lyon,*
Ecole Centrale de Lyon/Université Lyon 1/INSA de Lyon, ECL, 36 Avenue Guy de Collongue, 69134 Ecully Cedex, France

Keywords:
A1. segregation; A1. directional solidification; A1. convection; A1. boundary layer; A1. scaling analysis

Abstract
The objective of the present paper is to study the ability of an order of magnitude analysis [1] to give a realistic picture of segregation patterns in vertical *Bridgman* configurations, on the basis of hydrodynamic simulations. The scaling analysis leads to an analytical formulation of the solute boundary layer, involving the wall-shear stress at the solid/liquid interface. In order to test this analytical model, transient simulations of solute segregation in a 2D lid driven cavity configuration have been performed. The developed analytical model, which involves a quasi-steady approximation, is in good agreement with the numerical time-dependent results. The key results of this work are the correlation of segregation patterns in the solid with flow patterns in the liquid and the ability of the analytical model to describe lateral segregations and to capture unsteadiness in the limit of slow variations associated with *Bridgman* configurations.

1. Introduction

General background

Regarding the production of silicon for photovoltaic applications, the control of solute or impurities concentrations remains an important issue for solar cells efficiency. In a context of costs reduction and environmental protection, the development of alternative silicon purification processes based on metallurgical operations is a promising research area [2]. Metallic impurities, which usually have a very low partition coefficient k_0 [3], can be removed by segregation during a directional solidification process. However, the efficiency of the process would depend on the convective transport in the melt. Several stirring techniques, such as traveling or rotating magnetic fields [4]–[6], acoustic streaming [7]–[9] or mechanical stirring [10], can then be thought of to achieve a well-mixed melt and thus have an effective partition coefficient k_{eff} close to k_0.

Solute segregation during solidification processes has been widely investigated in the past decades, since the introduction of the convecto-diffusive parameter by Burton et al. [11] and the definition of the solute boundary layer thickness by Wilson [12]. In this area, numerical simulations can provide useful information for both physical understanding and industrial processes optimization. Nevertheless, the complete resolution of the directional solidification problem, coupling furnace thermal conditions, melt flow hydrodynamic and solute transport, remains a difficult task. As a consequence, any parametric optimization would require very heavy numerical means over very long computational time. This issue is linked to the variety of length scales involved, ranging from the meter for industrial crucibles (for instance, 800 kg G6 scale silicon ingots dimensions are 100x100x34 cm), to micrometers for the solute boundary layer thickness.

State of the art

Previous studies have demonstrated that scaling analyses can be useful for the understanding of solute segregation phenomena. These approaches are not meant to give accurate quantitative results, but they can describe the relative influence of the process parameters without performing the full computation of the solute transport. Then it is possible to achieve efficient simulations for full parametric studies. Recent publications investigate the ability of a scaling analysis model for the solute boundary layer proposed by Garandet et al. [1]. This model uses the wall-shear stress τ at the

solid/liquid interface as an indicator of the convection intensity for the solute transport in the vicinity of the growth front. Then it should be noted that this analytical model is dedicated to sharp solid/liquid interface solidification configurations, and is not relevant when a mushy zone or a dendritic growth is involved. The original publication [1] was dedicated to the validation of the model for a 2D lid driven cavity configuration in a steady-state regime. It was shown that using the average interface shear stress, the analytical model could give a good estimation of the solute boundary layer thickness, confirming the ability of the scaling analysis to capture the physics of the segregation phenomena.

More recently, Kaddeche et al. [13] compared this model with numerical and experimental results of solute segregation in the horizontal *Bridgman* configuration. Their aim was to test the model in a configuration with a reliable data base of numerical and experimental results. The flow was induced by natural convection, controlled by thermal buoyancy effects. The analytical model was found to be in good agreement with both numerical and experimental data.

Present study

In this frame of work, some questions remain concerning the applicability of the model for transient convection and/or solidification rate conditions, given that the scaling procedure involves a quasi-steady approximation. Our purpose is to complete the precedent studies for the validation of this segregation model. Therefore, we extend the lid driven cavity model presented in [1] to a transient configuration. We also investigate the ability of the analytical model to describe lateral segregations resulting from non-uniform convection conditions along the solid/liquid interface. The present work focuses on the example of silicon, keeping in mind that the results could be extended to other semiconductors or metals. Section 2 is dedicated to the description of the lid driven cavity configuration and related equations. Section 3 presents the numerical results obtained by transient simulations of solute segregation. A comparison with the analytical model is performed in section 4. Finally, we discuss in section 5 the case of unsteady solidification velocity.

2. Problem description

General principle

The present study focuses on the numerical simulation of solute segregation in a 2D lid driven cavity configuration. This configuration is a well-known canonical forced convection flow, in which the stirring intensity is characterized by a single dimensionless parameter, namely the *Reynolds* number ([22]–[24]). As a consequence, it is very appropriate for parametric studies. A similar study has already been presented by Garandet et al. [1] for a quasi-steady regime. Here we extend this numerical model in a transient regime in order to compute the solute concentration incorporated in the solid phase and study the influence of unsteady convection regimes. Figure 1 illustrates the problem configuration and defines the lid velocity V_L and the solidification rate V_I. To be consistent with the previous study we considered a cavity of width $L = 0.2\ m$. At the initialization the liquid height was $H(t_0) = 0.18\ m$.

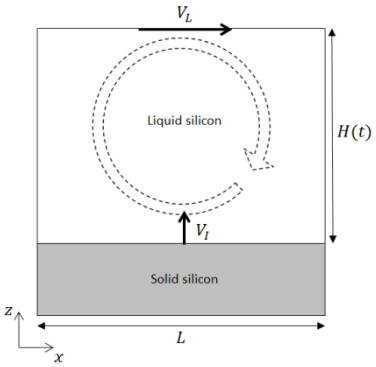

Figure 1 - Problem definition (geometry, interface velocity, lid velocity and schematic flow pattern).

Segregation concepts

Regarding purification by directional solidification, the key parameter to estimate the efficiency of the process is the thickness of the solute boundary layer δ at the solid/liquid silicon interface. A definition of this solute boundary layer thickness was given by Wilson [12]:

$$\delta = \frac{C_L^I - C_L^\infty}{-(\partial C_L/\partial z)_I}, \tag{1}$$

where C_L^I refers to the solute concentration in the liquid phase at the solid/liquid interface, C_L^∞represents the bulk concentration far from the interface and z is the normal to the interface. If we consider the case of a purely diffusive regime, δ is given by the ratio between the molecular diffusivity D and the solidification rate V_I. Then we can introduce the classical convecto-diffusive parameter Δ as a dimensionless boundary layer thickness [14]:

$$\Delta = \frac{\delta V_I}{D}. \tag{2}$$

This parameter was found to be a convenient way to estimate the efficiency of the convective transport in comparison to the diffusion. Indeed, a strong convection will result in a thin boundary layer, with Δ tending to 0. At the opposite, if Δ tends to 1, the solute transport is controlled by diffusion and the convection intensity is too low to reduce δ. If we consider the solute conservation at the interface, assuming negligible diffusion at solid state:

$$-D\left.\frac{\partial C_L}{\partial z}\right|_I = V_I(1-k_0)C_L^I, \tag{3}$$

we can express Δ by the following relation:

$$\Delta = \frac{C_L^I - C_L^\infty}{(1-k_0)C_L^I}. \tag{4}$$

An interesting feature of Wilson's definition of the solute boundary layer thickness [12] is that it allows to determine unambiguously the effective partition coefficient k_{eff} using Δ:

$$k_{eff} = \frac{C_S^I}{C_L^\infty} = \frac{k_0}{1-(1-k_0)\Delta}. \tag{5}$$

One of the main issues for the numerical simulation of solute segregation is the accurate description of the solute boundary layer. This point becomes challenging for the simulation of silicon purification by a directional solidification process, given that the objective is to ensure that Δ is small enough so that k_{eff} remains close to k_0 in order to get an efficient segregation. The necessity to resolve such a fine solute boundary layer requires a very fine mesh at the solid/liquid interface, which is not always compatible with simulations of solidification processes in industrial purification furnaces, for instance at the G5 or G6 scale. To address this problem, an analytical formulation of δ derived from a scaling analysis has been proposed by Garandet et al. [1] in a steady state configuration. This formulation uses the wall-shear stress τ at the solid/liquid interface to measure the convection intensity and evaluate δ. In this context, our numerical model is used as a test case for the validation of this analytical model in transient configurations.

General equations

To compute this problem we use the commercial code ANSYS FLUENT [15]. To define the lid driven cavity flow we resolve mass and momentum conservation equations, given by the following relations for an incompressible flow:

$$\nabla.\vec{u} = 0, \tag{6}$$

$$\frac{\partial \vec{u}}{\partial t} + (\vec{u}.\nabla)\vec{u} = -\frac{1}{\rho}\nabla P + \frac{1}{\rho}\nabla.[(\mu+\mu_t)\nabla\vec{u}], \tag{7}$$

where $\vec{u}$, P, ρ and μ respectively stand for the fluid velocity, the pressure, the density and the dynamic viscosity. μ_t denotes the turbulent dynamic viscosity in a *Reynolds Averaged Navier-Stokes* framework. The solute conservation in the liquid phase is given by:

$$\frac{\partial C_L}{\partial t} + (\vec{u}.\nabla)C_L = \nabla.[(D + D_t)\nabla C_L]\,, \tag{8}$$

where C_L represents the solute mass fraction in the liquid and D_t stands for the turbulent diffusion coefficient which accounts for the influence of turbulence on the solute transport [15]. The interface concentration in the solid C_S^I is computed thanks to the partition coefficient k_0 by the relation:

$$C_S^I = k_0 C_L^I\,. \tag{9}$$

In order to study the influence of the convection on the segregation we define different convective regimes ranging from purely diffusive to fully turbulent. To characterize these different regimes we use the *Reynolds* number based on the cavity width, $Re_L = (V_L L)/\nu$, varying from 0 to 10^6 in the present study. For turbulent regimes ($Re_L \geq 10^4$) we use the two equations turbulence model $k-\varepsilon$ *realizable* proposed by FLUENT, associated with the "*Enhanced Wall Treatment*" for hydrodynamic boundary layers computation. The "*Enhanced Wall Treatment*" uses a two-layer approach in order to adapt the turbulence model in the near-wall region, depending on the value of a wall-distance-based turbulent *Reynolds* number [15]. Then, if the first cell adjacent to the wall is thinner than the hydrodynamic viscous sublayer, the near wall flow is computed with a laminar model. Otherwise, a classic logarithmic wall function is used to define the velocity profile in the first cell. A blending function is used to ensure a smooth transition between the two formulations.

Main assumptions and boundary conditions

Regarding boundary conditions, we impose the lid velocity at the top of the cavity and no slip conditions on the lateral walls. As a consequence the velocity is $V_L\vec{x}$ at the top lid and zero on the lateral walls. To simulate the directional solidification process we impose a solidification velocity $V_I\vec{z}$ at the solid/liquid interface. We model this interface as a plane wall with no slip condition. The decrease in the amount of liquid while the interface moves upwards is accounted for by setting a mass sink at the interface. As explained in former works ([1], [16], [17]), the definition of this mass sink leads to the definition of equivalent source terms for the other variables of the problem. For the solute concentration, the source term is multiplied by the partition coefficient k_0, leading to the formation of the solute boundary layer in the liquid. In the present work, the diffusion of the impurities in the solid is neglected and the densities of the liquid and the solid phases are assumed to be equal.

Mesh requirements and convergence criteria

A structured mesh with a cell size of 2x2 mm away from the interface was used. The mesh is refined in the liquid part at the solid/liquid interface to account for the solute boundary layer. The first cell adjacent to the interface is $5\,\mu m$ high which is ten times smaller than the typical solute boundary layer thickness obtained for the highest convective regime, namely $Re_L = 10^6$. Then the computation grid contains 13400 cells. The dynamic mesh options proposed by FLUENT are used to define the motion of the solid/liquid interface and adapt the mesh consequently at each time-step with a layering procedure. The time-step amplitude is defined to get a constant interface displacement at each time-step. In the case of a constant solidification rate of $10^{-5}\,m/s$, the time-step amplitude is set at 100 s in order to get an interface displacement of 1 mm.

The influence of spatial and temporal discretization is checked with a test computation. For this test a new mesh is defined with a cell size of 0.5x0.5 mm away from the interface, resulting in a 168000 cells grid since the interface refinement is conserved. The time-step amplitude is set at 50 s in order to impose an interface displacement of 0.5 mm at each time-step. A segregation simulation is performed with this numerical configuration for the turbulent case $Re_L = 10^4$. The two numerical configurations lead to identical results for fluid velocity, interface shear stress and solute concentration. For instance, the comparison of the solute concentration profiles in the solid leads to

a mean relative deviation of 2.7% between the two configurations and the mean relative deviation for velocity profiles in the liquid is about 3.4%. Then we consider that spatial and temporal discretization is sufficient for the computation of the flow, the solute transport and local gradients at the interface. Regarding convergence criteria, residuals decrease and solute conservation in solid and liquid phases are checked at each time-step.

3. Numerical results

As mentioned previously, the influence of the convective regime is investigated by imposing different lid velocities. At first, for validation and comparison purposes, we consider the ideal case of the purely diffusive regime, imposing $V_L = 0$ at the lid. Then two laminar flows are simulated for $Re_L = 10^2$ and 10^3. Finally three turbulent flows are treated for $Re_L = 10^4$, 10^5 and 10^6. For this hydrodynamic study we consider a partition coefficient $k_0 = 0.3$ and a diffusion coefficient $D = 10^{-8}\, m^2.s^{-1}$ for the solute, in order to be consistent with the previous work [1]. The initial concentration in the liquid is set at $C_0 = 20\, ppmw$ (part per million weight). As it is often the case for solar grade silicon, the solute concentration is sufficiently low to consider constant hydrodynamic properties for the silicon melt, with a density $\rho = 2550\, kg.m^{-3}$ and a dynamic viscosity $\mu = 7.5\, 10^{-4}\, Pa.s$. The solidification velocity is fixed at $V_I = 10^{-5} m.s^{-1}$, which is the order of magnitude for silicon purification processes. The computations are performed until the solid fraction reaches 89%.

For Re_L ranging from 10^2 to 10^6, the flow features a main recirculation and secondary vortices located in the corners, as illustrated on Figure 2.A. These vortices induce characteristic points, defined by the location where the wall-shear stress is zero on the solid/liquid interface (Figure 2.B). Here we must distinguish the points where the flow is impinging the interface, resulting in a strong convective transport, and the points where the flow is leaving the interface, referred to as separation points in the following. At separation points the convective transport is reduced, which leads to solute accumulation and a locally thicker solute boundary layer. The extent of the vortices is mainly controlled by the magnitude of the lid velocity. However, the continuous reduction of the liquid height H also influences the flow topology. As a result, the positions of the impingement and separation points evolve during the solidification process.

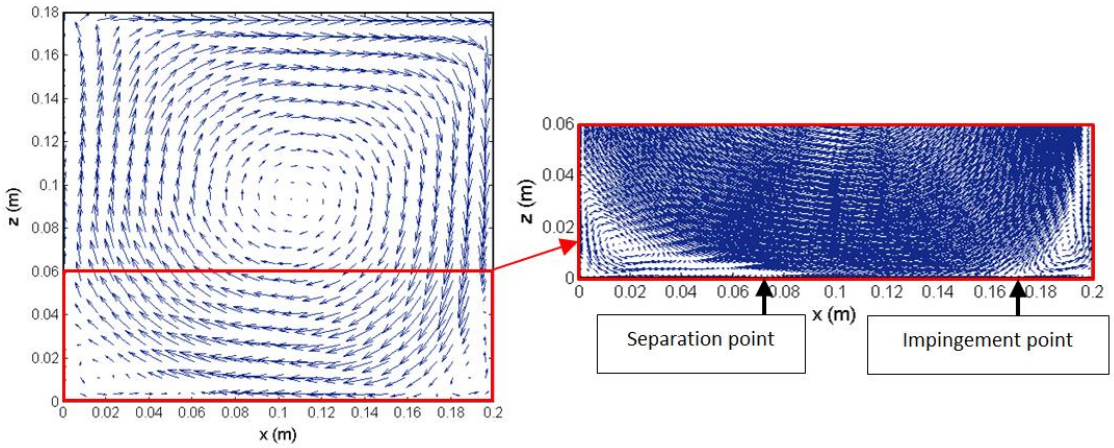

(A) velocity field (B) secondary vortices

Figure 2 - Velocity field for $\boldsymbol{Re_L = 10^4}$ (A) and illustration of the separation point associated with the lower left corner secondary vortex and the impingement point at the lower right corner (B).

Figure 3 presents color-maps of the solute concentration in the solid obtained from the transient simulations. We can see for the diffusive regime (Figure 3.A, $Re_L = 0$) that the concentration is x-independent and increases with z in the first tenth of the ingot height. In the rest of the ingot the concentration remains equal to the nominal concentration C_0, as expected from the analytical solution of the purely diffusive regime [18]. For Re_L ranging from 10^2 to 10^5 (Figure 3.B, C, D and E)

we can observe important concentration variations in the horizontal direction. These lateral segregations are directly related to a non-uniform convection at the solid/liquid interface (i.e. secondary vortices and separation points). For $Re_L = 10^6$ (Figure 3.F) we can see that the concentration is almost uniform in the horizontal direction, which means that the convection is strong enough on the whole cavity width to ensure a constant boundary layer thickness.

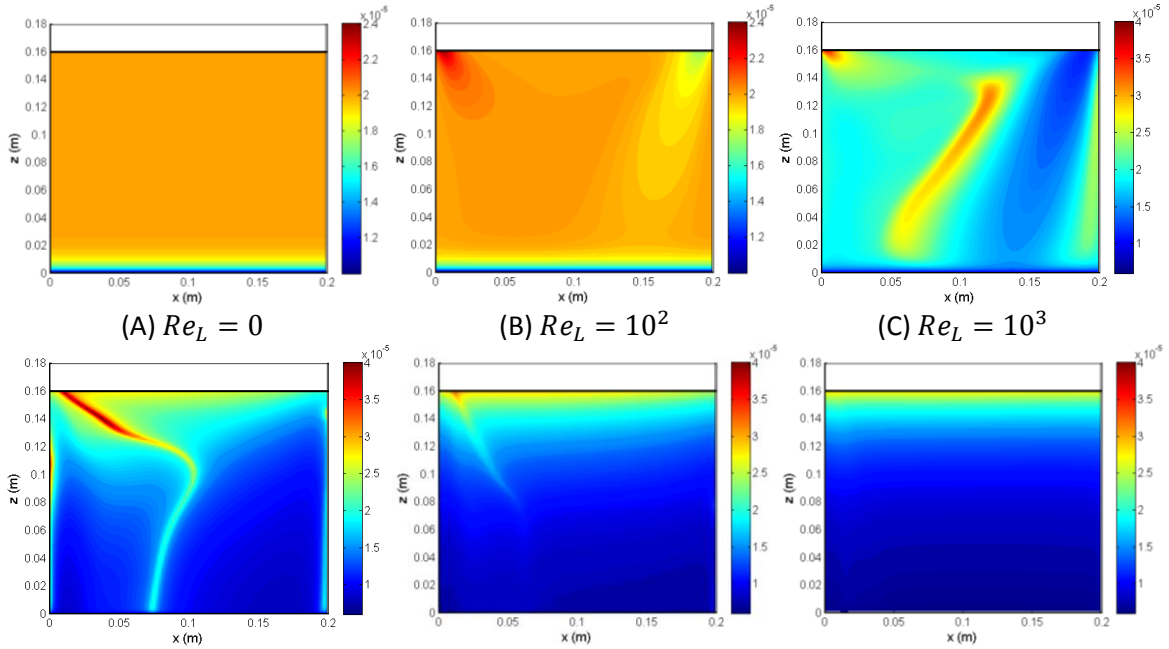

(A) $Re_L = 0$ (B) $Re_L = 10^2$ (C) $Re_L = 10^3$

(C) $Re_L = 10^4$ (D) $Re_L = 10^5$ (E) $Re_L = 10^6$

Figure 3 - Color-maps of solute mass fraction in the solid phase obtained from the transient simulations at *Reynolds* numbers of: 0 (A), 10^2 (B), 10^3 (C), 10^4 (D), 10^5 (E) and 10^6 (F). Different color scales are used in order to enhance contrast.

The abscissas of impingement and separation points have been extracted at several time-steps from the transient simulations. The paths followed by these locations during the solidification of the ingot are symbolized in Figure 4 over selected color-maps from Figure 3. As we can see on Figure 4.A (laminar flow, $Re_L = 10^3$) and on Figure 4.B and C (turbulent flows, $Re_L = 10^4$ and 10^5), for a given height in the ingot, the maximum concentration in the solid is located at the separation point of the main recirculation of the flow. This clearly highlights the direct correlation between the flow structure and the concentration field obtained in the solid.

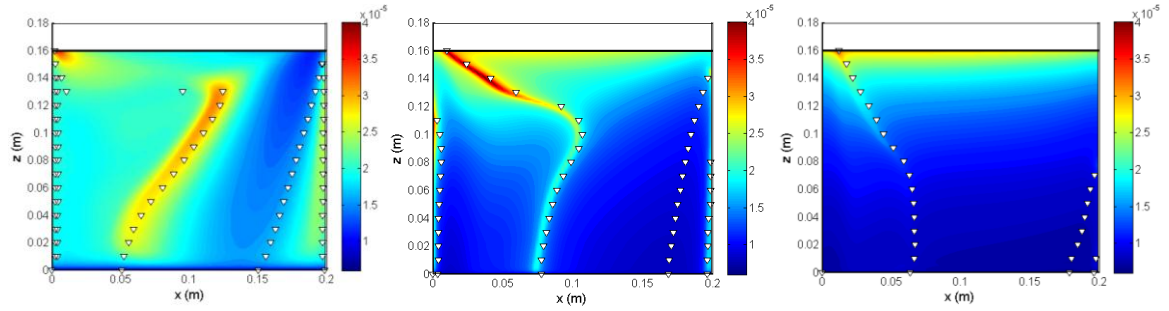

(A) $Re_L = 10^3$ (B) $Re_L = 10^4$ (C) $Re_L = 10^5$

Figure 4 - Correlation between separation and impingement points at the solid/liquid interface (white symbols) and lateral solute segregations in the solid, for *Reynolds* numbers of 10^3 (A), 10^4 (B) and 10^5 (C).

Longitudinal segregation profiles are presented in Figure 5. The notation $\langle C_S \rangle$ refers to span averaged concentrations in the horizontal direction. The analytical reference solutions for the diffusive regime and *Scheil*'s law [18] are plotted in solid lines. The numerical results for laminar flows tend to the diffusive regime solution, showing a uniform span averaged concentration equal to C_0, after an initial transient necessary for the formation of the solute boundary layer. For turbulent flows, the results tend to *Scheil*'s relation, with an effective partition coefficient k_{eff} getting closer to k_0 as the convection increases.

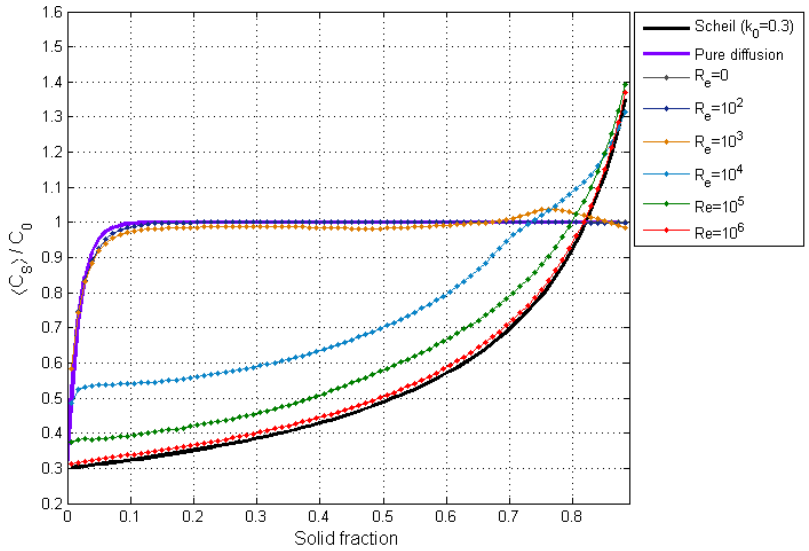

Figure 5 - Normalized span averaged concentration profiles in the solid obtained by transient simulations for the different regimes and analytical solutions for pure diffusion and *Scheil* regimes.

4. Analytical approach

Scaling analysis

In this section we present a comparison of our numerical results and the scaling analysis presented in [1]. We shall recall the main steps of this analysis; the reader can refer to previous publications [1] and [14] for a complete description. First it has been shown that the steady state scaling of equation (8) leads to the following equation for δ:

$$\frac{D}{\delta} = V_I - w(\delta)\,, \tag{10}$$

where D stands for the molecular diffusivity, as defined earlier, and $w(\delta)$ is the vertical component of the convection velocity, taken at the coordinate $z = \delta$. In order to solve this equation, one should define this convection velocity. Assuming at first order a linear profile for the tangential velocity u at the vicinity of the solid/liquid interface and introducing the wall-shear stress τ at the interface, we can write:

$$u(z) \sim \frac{\tau}{\mu} z\,, \tag{11}$$

where μ represents the molecular dynamic viscosity. Then, as detailed in [1], using continuity and taking the cavity width L as the length scale for the variations of u along the interface, one gets the following expression for w:

$$w(z) \sim -\frac{\tau}{\mu L} z^2\,. \tag{12}$$

Combining equations (10) and (12), we get a third order equation for δ:

$$\frac{D}{\delta} = V_I + \frac{\tau}{\mu L}\delta^2\,. \tag{13}$$

This equation can be solved analytically, resulting in the expression of the convecto-diffusive parameter Δ_{th} as a function of a unique dimensionless parameter $B = (\tau D^2)/(V_l^3 \mu L)$:

$$\Delta_{th} = (2B)^{-1/3} \left\{ \left(1 + \sqrt{1 + \frac{4}{27B}} \right)^{1/3} + \left(1 - \sqrt{1 + \frac{4}{27B}} \right)^{1/3} \right\}. \quad (14)$$

As explained in [1], this formulation presents two asymptotic regimes. When B tends to zero, Δ_{th} tends to 1, corresponding to a diffusive regime. When B becomes much larger than 1, representing convective regimes, Δ_{th} tends to $B^{-1/3}$.

Comparison with numerical results

Figure 6 presents local values of wall-shear stress and convecto-diffusive parameter along the solid/liquid interface in laminar ($Re_L = 10^3$) and turbulent ($Re_L = 10^5$) regimes. These values are arbitrarily taken at a solid fraction of 44%; we have checked that results obtained for different solid fractions present similar features, so that this picture can be considered as representative of typical results all along the solidification process. The numerical convecto-diffusive parameter Δ_{num} is computed from solute concentrations by relation (4) and the analytical convecto-diffusive parameter Δ_{th} is directly computed by relation (14), using the numerical results for τ. For both laminar and turbulent regimes we can see a clear negative correlation between τ and Δ_{num}, with a maximum solute boundary layer thickness localized near the separation point of the main recirculation (where $\tau(x_s) = 0$).

Regarding the values of Δ_{th} provided by the scaling analysis, we find good qualitative agreement with the numerical solution for the turbulent regime (Figure 6.D). In fact, it is interesting to observe that the scaling analysis, which uses a one-dimensional hypothesis (equation (10)), can provide useful insights regarding local variations for the solute boundary layer. This result confirms that the wall-shear stress at the solid/liquid interface is a very good indicator of the convective transport, not only for averaged values as it was shown by precedent studies ([1], [13]) but also for local variations of the convective transport. This support the fact that the analytical model could be an efficient way to estimate the variations of the interface composition Δ along the solid/liquid front when the convection is not uniform and leads to lateral segregations. However, attention should be paid for flow separation points where the analytical model strongly overestimates the solute boundary layer thickness. This issue is directly related to the assumption of a parallel flow in the viscous sublayer to define a linear velocity profile in the solute boundary layer (equation (11)). For separation and impingement points, it is clear that this approach loses its validity. For the laminar case (Figure 6.C), let us recall that on average the solute transport is mainly diffusive with an average Δ close to 1, see Figure 5. In this configuration lateral segregation is very important, as seen on Figure 3.C, and the scaling procedure is not adapted to account for such concentration gradients in the horizontal direction, even though it is able to reproduce qualitatively some features of the Δ variations. For example, we can see that the analytical model is unable to predict a convecto-diffusive parameter locally larger than 1, as observed in the numerical simulations, since Δ_{th} can not exceed 1 when B tends to zero. However, the relative difference between the numerical and the analytical solutions remains under 20% which is reasonable for a scaling analysis.

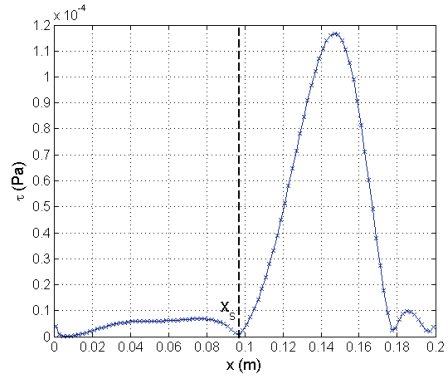

(A) Wall-shear stress, $Re_L = 10^3$

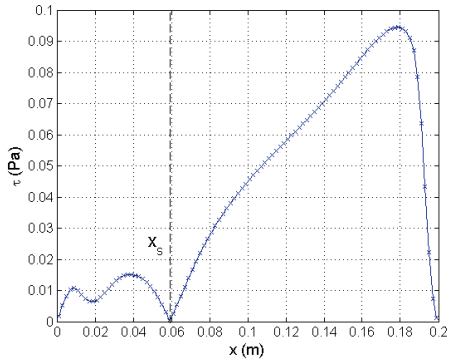

(B) Wall-shear stress, $Re_L = 10^5$

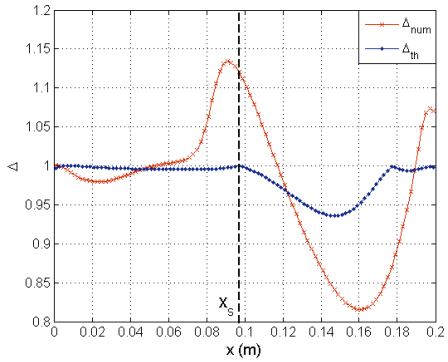

(C) Convecto-diffusive parameter, $Re_L = 10^3$

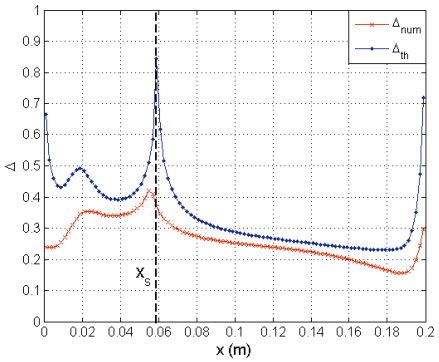

(D) Convecto-diffusive parameter, $Re_L = 10^5$

Figure 6 - Wall-shear stress and convecto-diffusive parameter at the solid/liquid interface, comparison between numerical (Δ_{num}) and analytical (Δ_{th}) results.

As explained in section 3, the dynamics of the solidification process can lead to an unsteady convective flow. In our case, flow variations are caused by the reduction of the liquid height. To characterize these variations and their influence on segregation we can compute span averaged values $\langle\tau\rangle$, $\langle\Delta\rangle$ and $\langle\Delta_{th}\rangle$ along the solid/liquid interface and study their evolution during the solidification. We can see on Figure 7.A and B the variation of $\langle\tau\rangle$ for laminar and turbulent regimes during the solidification process. This evolution induces a variation of the solute boundary layer thickness (Figure 7.C). The agreement between numerical and analytical values of $\langle\Delta\rangle$ for both laminar and turbulent regimes is quite good. Then, it appears that a meaningful estimate of Δ can be found using instantaneous values of the interface shear stress. In fact, we can see that the flow variations occur at a time scale comparable to the solidification time of the ingot, i.e. $16\,10^3\ s$. Therefore, these variations can be considered as slow compared to the diffusion time at the scale of the solute boundary layer [19]. This diffusion time is given by the ratio δ^2/D and is about 94 s for the laminar case $Re_L = 10^3$ and 7 s for the turbulent case $Re_L = 10^5$. This argument confirms the validity of the quasi-steady hypothesis used in the scaling analysis. As we can see on Figure 7.C, the computation of $\langle\Delta_{th}\rangle$ with the instantaneous value of $\langle\tau\rangle$ leads to a similar variation as observed for $\langle\Delta_{num}\rangle$ in the turbulent regime ($Re_L = 10^5$). Then the analytical model seems valid to describe the influence of slow variations in the convection regime when the solute transport remains mainly convective.

For the laminar regime (Figure 7.C, $Re_L = 10^3$), we can see that the variation of $\langle\Delta_{num}\rangle$ is also consistent with the evolution of $\langle\tau\rangle$ and $\langle\Delta_{th}\rangle$, except for a solid fraction between 70% and 80%. At this location, the local increase of $\langle\Delta_{num}\rangle$ corresponds to a modification of the flow topology, when the secondary vortex is confined and collapses. The solute transport being mainly diffusive, the solute repartition in the liquid is not homogeneous and the secondary vortex is more concentrated than the main recirculation. Then, as the secondary vortex gets more and more confined, the concentrated liquid is mainly transported to the interface resulting in an increase of the solute

boundary layer thickness. This phenomenon can be described as a transient lateral segregation. An animation of the solute transport in the liquid for this configuration can be found in the online version of the paper [20].

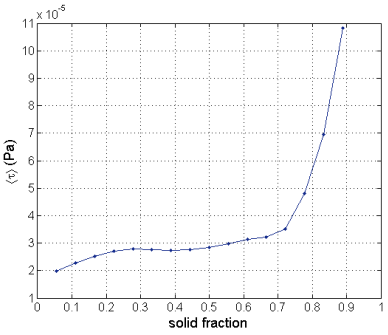

(A) Wall-shear stress, $Re_L = 10^3$

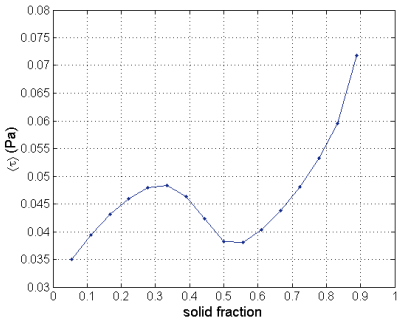

(B) Wall-shear stress, $Re_L = 10^5$

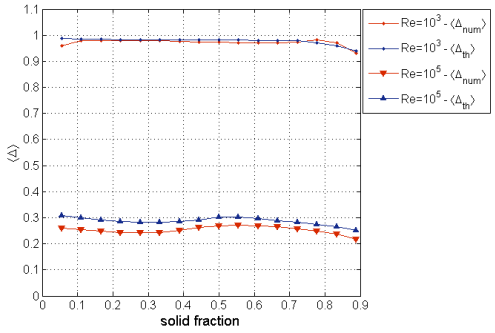

(C) Convecto-diffusive parameter

Figure 7 - Span averaged wall-shear stress and convecto-diffusive parameter at the solid/liquid interface as a function of the solid fraction, for *Reynolds* numbers of 10^3 and 10^5.

At this point it appears interesting to compare our numerical results with the previous results in quasi-steady regime [1]. To do so, we report on Figure 8 the values of $\langle\Delta\rangle$ for the different regimes ($Re_L = 10^2$ to 10^6), obtained for different solid/liquid interface positions varying from 1 cm to 16 cm and referred to as Δ_{dyn}. These data are acquired at each centimeter and the equivalent solid fractions lie between 5.6% and 89%. Values for $\langle B\rangle$ were computed from the span averaged values of wall-shear stress at the solid/liquid interface. We also plot the results obtained by the quasi-steady model in [1], referred to as Δ_{stat}, for the same configuration ($V_I = 10^{-5} m.s^{-1}$ and $D = 10^{-8} m^2.s^{-1}$). As we can see, both steady and unsteady simulations follow the same law for the solute boundary layer thickness. This tends to confirm the validity of the quasi-steady approximation for this configuration. The analytical solution, given by relation (14), is plotted in dashed line. The precedent study [1] already pointed out the good agreement with numerical results for diffusive regimes up to the convecto-diffusive transition. The divergence for fully convective regime was attributed to the assumptions used for the expression of $w(z)$ by equation (12). It should be noted that this presentation of the results, based on averaged values, is well adapted for a global estimation of the segregation process efficiency but does not reflect the presence of local variations linked to lateral segregations and unsteady convective transport.

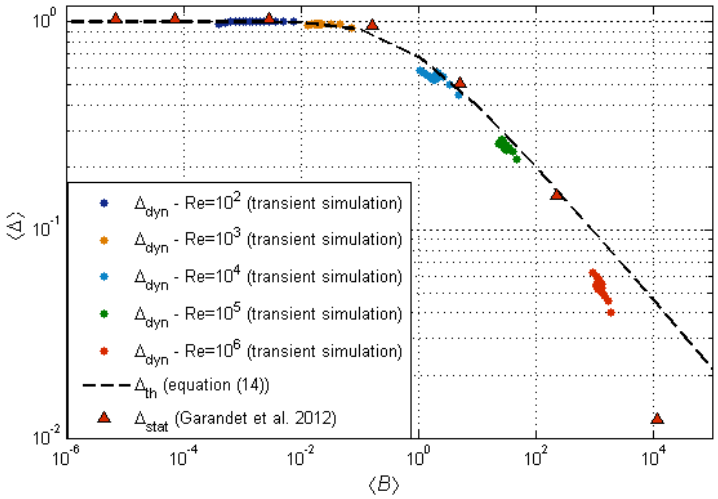

Figure 8 - $\langle\Delta\rangle$ as a function of $\langle \boldsymbol{B} \rangle$. Comparison between transient simulations, quasi-steady simulations [1] and analytical model (14).

5. Unsteady solidification velocity

Objective and configuration

Up to now, we have been studying unsteady convection conditions but for a constant solidification rate. However, during directional solidification processes, the solidification velocity can present some fluctuations. Given that the solidification rate is mainly controlled by the thermal conditions in the furnace, the inertia of the process is expected to limit the fluctuations to low frequencies, as opposed e.g. to *Czochralski* growth where the frequency of the pulling speed variations can be quite high. In the following, 'high' and 'low' frequencies should be understood with reference to the time scale of diffusion processes taking place at the boundary layer thickness scale. In this section we intend to discuss the validity of the scaling analysis of section 4 when the solidification rate exhibits slow variations.

The analysis of periodical oscillations of the solid/liquid interface velocity in solidification processes has already been performed analytically [19] and numerically [21], [25]. These studies highlighted the existence of a low frequency regime where the quasi-steady approximation is valid. This regime occurs when the variations of the interface velocity are slow enough for the solute boundary layer to adapt instantaneously. The frequency regime can be characterized by the dimensionless parameter $Fq = (\omega\bar{\delta}^2)/D$, ω being the pulsation of the oscillations and $\bar{\delta}$ the solute boundary layer thickness in the case of a constant interface velocity [19]. The transition between the low and high frequency regimes is at $Fq = 1$, and the low frequency limit is obtained when Fq tends to zero. When Fq increases the concentrations fluctuations are expected to lag behind the velocity fluctuations, with a phase shift dependent on the value of Fq.

Given that the scaling procedure is based on a quasi-steady approximation, the analytical model is expected to hold in the low frequency regime only. In order to check the validity of the model in this particular regime, we implement a periodical fluctuation of the solidification velocity $V_I(t)$ in our numerical model, defined by the following relation:

$$V_I(t) = \overline{V_I}(1 + \alpha \sin(\omega t)) \,, \qquad (15)$$

$\overline{V_I}$ being the average velocity and α the amplitude of the oscillations. For this test we use the configuration of the convective regime $Re_L = 10^6$. Then, using the results presented on Figure 8, we can estimate the average solute boundary layer thickness $\bar{\delta} \approx 52\ \mu m$ for a constant solidification rate. We define a period $T = 2000\ s$ for the velocity fluctuations, resulting in $Fq \approx 8.5 * 10^{-4}$. If we consider the analytical results presented by Garandet [19], such a low frequency regime should lead to an almost null phase shift between growth rate and concentration fluctuations. The average

velocity is kept at $\overline{V_I} = 10^{-5}\ m.s^{-1}$ and we define the oscillations amplitude $\alpha = 0.5$, a significant value.

Results and discussion

Figure 10 presents the fluctuations of the normalized span averaged concentration $\langle C_n \rangle$ in the solid, defined by the following equation:

$$\langle C_n \rangle = \frac{\langle C_s \rangle - \langle \overline{C_s} \rangle}{\langle \overline{C_s} \rangle}, \tag{16}$$

$\langle \overline{C_s} \rangle$ being the average concentration of the solid at the solid/liquid interface obtained for a constant solidification velocity. We can see that concentration fluctuations are in phase with velocity fluctuations, confirming the low frequency regime (Figure 9 and Figure 10). It is also interesting to observe that even though the $\langle C_n \rangle$ oscillations have similar amplitude, a significant variation is apparent. To explain this point we have to recall that the amplitude depends on the convecto-diffusive parameter $\langle \bar{\Delta} \rangle$ in the case of constant solidification rate [19]. In our configuration, because of unsteady convective transport, $\langle \bar{\Delta} \rangle$ is varying during the process (Figure 7). This is the reason for the non-constant amplitude of $\langle C_n \rangle$ oscillations. Now, if we consider the analytical formulation of the low frequency regime we can get an estimation of the longitudinal segregation oscillations [19]. The amplitude of the oscillations, referred as $|\langle C_n \rangle|$, is given by the relation:

$$|\langle C_n \rangle| = 2\alpha \frac{(1-k_0)\langle \bar{\Delta} \rangle (1 - \langle \bar{\Delta} \rangle)}{1 - (1-k_0)\langle \bar{\Delta} \rangle}. \tag{17}$$

Taking the time averaged value of $\langle \bar{\Delta} \rangle \sim 0.052$, we get $|\langle C_n \rangle| \sim 0.036$ which is consistent with the amplitude observed in the numerical simulation (Figure 10). Finally, Figure 11 compares the fluctuations of the span averaged convecto-diffusive parameters $\langle \Delta_{num} \rangle$, given by the numerical simulation, and $\langle \Delta_{th} \rangle$ calculated with the span averaged wall-shear stress $\langle \tau \rangle$ and the instantaneous velocity $V_I(t)$. For comparison purpose, these parameters are normalized by their respective values $\langle \overline{\Delta_{num}} \rangle$ and $\langle \overline{\Delta_{th}} \rangle$ obtained with a constant solidification rate. We can see that the oscillatory signals have almost constant amplitude, which is also in agreement with the analytical formulation of the low frequency regime for the present configuration [19]. Besides, the two oscillatory signals for $\langle \Delta_{num} \rangle$ and $\langle \Delta_{th} \rangle$ have the same amplitude and present a very slight phase shift. This result confirms that the analytical model can accurately predict the oscillations of the solute boundary layer thickness for low frequency perturbations encountered in *Bridgman* processes.

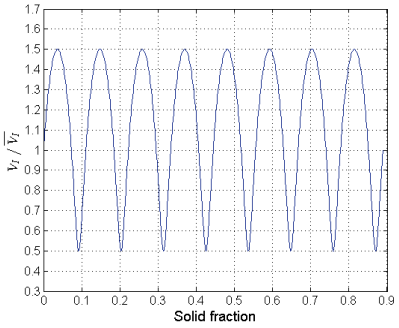

Figure 9 - Normalized solidification rate.

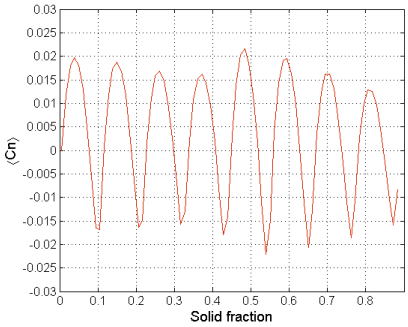

Figure 10 - Normalized solute concentration $\langle \boldsymbol{C_n} \rangle$ in the solid.

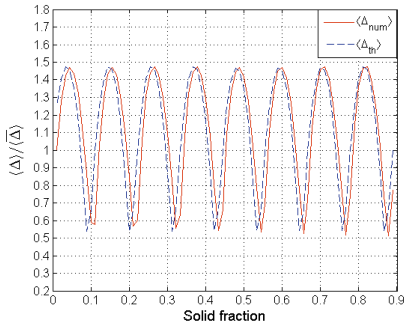

Figure 11 - Normalized convecto-diffusive parameter ⟨Δ⟩;
numerical and analytical results.

6. Conclusion

Transient simulations of solute segregation in a 2D lid driven cavity have been performed. The results compare well with the quasi-steady simulations presented in [1]. The model is used as a test case for an analytical formulation of the solute boundary layer based on a scaling analysis and involving the wall-shear stress at the solid/liquid interface. The transient simulations enable us to investigate the ability of the analytical model to give a correct estimation of the convecto-diffusive parameter Δ in the case of unsteady convection and solidification rate conditions. The comparison with numerical results shows that the analytical model can provide a good estimation of Δ and his variations for slow variations of the convective regime and low frequency fluctuations of the solidification rate. The model is tested in a low frequency regime, in the quasi-steady assumption framework, which is not highly restrictive as far as *Bridgman* growth is concerned. Another interesting feature of the analytical model is its ability to estimate local variations of Δ along the solid/liquid interface when the convection is not uniform. However, special attention should be paid regarding separation points and strong transient lateral segregation.

The main benefit of this analytical approach is to suppress the need for very fine mesh in the solute boundary layer. This feature seems especially interesting for solidification computations by implicit methods (like the enthalpy-porosity formulation proposed in ANSYS FLUENT) where the position of the interface is not explicitly known, making local refinement of the mesh quite difficult to perform. In our opinion, this model could be used for simulations of silicon purification and crystallization in industrial scale furnaces. With this effective approach, one could extract very useful information on boundary layer thickness and solute repartition in the solid from the resolution of the hydrodynamic and thermal problem. The reduction of the computation time would enable us to perform parametric studies for process optimization. The absolute accuracy of the results would remain limited by the scaling procedure but the relative influence of the process parameters could be obtained. Localized segregation variations related to non-uniform convection could be detected as well.

Acknowledgments

The authors warmly acknowledge J.P. Garandet for fruitful discussions on the subject.

References

[1] J. P. Garandet, N. Kaupp, D. Pelletier, and Y. Delannoy, “Solute segregation in a lid driven cavity: Effect of the flow on the boundary layer thickness and solute segregation,” *J. Cryst. Growth*, vol. 340, no. 1, pp. 149–155, 2012.

[2] J. Hofstetter, J. F. Lelièvre, C. del Cañizo, and A. Luque, “Acceptable contamination levels in solar grade silicon: From feedstock to solar cell,” *Mater. Sci. Eng. B*, vol. 159–160, pp. 299–304, 2009.

[3] F. A. Trumbore, “Solid Solubilities of Impurity Elements in Germanium and Silicon,” *Bell Syst. Tech. J.*, vol. 39, no. 1, pp. 205–233, 1960.

[4] P. Dold, A. Cröll, M. Lichtensteiger, T. Kaiser, and K. W. Benz, “Floating zone growth of silicon in magnetic fields: IV. Rotating magnetic fields,” *J. Cryst. Growth*, vol. 231, no. 1, pp. 95–106, 2001.

[5] I. Grants and G. Gerbeth, “Use of a traveling magnetic field in VGF growth: Flow reversal and resulting dopant distribution,” *J. Cryst. Growth*, vol. 310, no. 16, pp. 3699–3705, 2008.
[6] C. Tanasie, D. Vizman, and J. Friedrich, “Numerical study of the influence of different types of magnetic fields on the interface shape in directional solidification of multi-crystalline silicon ingots,” *J. Cryst. Growth*, vol. 318, no. 1, pp. 293–297, 2011.
[7] B. Moudjed, V. Botton, D. Henry, H. Ben Hadid, and J.-P. Garandet, “Scaling and dimensional analysis of acoustic streaming jets,” *Phys. Fluids*, vol. 26, no. 9, p. 093602, 2014.
[8] W. Dridi, D. Henry, and H. Ben Hadid, “Influence of acoustic streaming on the stability of melt flows in horizontal Bridgman configurations,” *J. Cryst. Growth*, vol. 310, no. 7–9, pp. 1546–1551, 2008.
[9] G. N. Kozhemyakin, L. V. Nemets, and A. A. Bulankina, “Simulation of ultrasound influence on melt convection for the growth of GaxIn1−xSb and Si single crystals by the Czochralski method,” *Ultrasonics*, vol. 54, no. 8, pp. 2165–2168, 2014.
[10] S. Dumitrica, D. Vizman, J.-P. Garandet, and A. Popescu, “Numerical studies on a type of mechanical stirring in directional solidification method of multicrystalline silicon for photovoltaic applications,” *J. Cryst. Growth*, vol. 360, pp. 76–80, 2012.
[11] J. A. Burton, R. C. Prim, and W. P. Slichter, “The distribution of solute in crystals grown from the melt. Part I. Theoretical,” *J. Chem. Phys.*, vol. 21, no. 11, pp. 1987–1991, 1953.
[12] L. O. Wilson, “On interpreting a quantity in the Burton, Prim and Slichter equation as a diffusion boundary layer thickness,” *J. Cryst. Growth*, vol. 44, no. 2, pp. 247–250, 1978.
[13] S. Kaddeche, J. P. Garandet, D. Henry, H. B. Hadid, and A. Mojtabi, “On the effect of natural convection on solute segregation in the horizontal Bridgman configuration: Convergence of a theoretical model with numerical and experimental data,” *J. Cryst. Growth*, vol. 409, pp. 89–94, 2014.
[14] J. P. Garandet, T. Duffar, and J. J. Favier, “On the scaling analysis of the solute boundary layer in idealized growth configurations,” *J. Cryst. Growth*, vol. 106, no. 2, pp. 437–444, 1990.
[15] ANSYS Inc., “ANSYS FLUENT 14.0 Theory Guide.” 2011.
[16] Y. Delannoy and K. Zaidat, “Modelling the segregation of impurities during solidification with turbulent electromagnetic stirring,” in *The 7 th International Conference on Electromagnetic Processing of Materials*, 2012, pp. 217–220.
[17] F. B. Santara, “Cristallisation du silicium photovoltaïque sous induction électromagnétique: étude d’une vanne de rétention et de la ségrégation sous brassage,” Ph. D. Thesis, Institut National Polytechnique de Grenoble-INPG, 2010.
[18] W. A. Tiller, K. A. Jackson, J. W. Rutter, and B. Chalmers, “The redistribution of solute atoms during the solidification of metals,” *Acta Metall.*, vol. 1, no. 4, pp. 428–437, 1953.
[19] J. P. Garandet, “Microsegregation in crystal growth from the melt: an analytical approach,” *J. Cryst. Growth*, vol. 131, no. 3–4, pp. 431–438, 1993.
[20] *See supplementary video - solute transport in a laminar flow - Re=1E3*. 2015.
[21] F. Z. Haddad, J. P. Garandet, D. Henry, and H. Ben Hadid, “Analysis of the unsteady segregation in crystal growth from a melt,” *J. Cryst. Growth*, vol. 204, no. 1–2, pp. 213–223, 1999.
[22] E. Erturk, T. C. Corke, and C. Gökçöl, “Numerical solutions of 2-D steady incompressible driven cavity flow at high Reynolds numbers,” *Int. J. Numer. Methods Fluids*, vol. 48, no. 7, pp. 747–774, 2005.
[23] E. Erturk, “Discussions on driven cavity flow,” *Int. J. Numer. Methods Fluids*, vol. 60, no. 3, pp. 275–294, 2009.
[24] U. Ghia, K. N. Ghia, and C. T. Shin, “High-Re solutions for incompressible flow using the Navier-Stokes equations and a multigrid method,” *J. Comput. Phys.*, vol. 48, no. 3, pp. 387–411, 1982.
[25] F. Z. Haddad, J. P. Garandet, D. Henry, and H. B. Hadid, “Analysis of the unsteady segregation in crystal growth from a melt Part II: Fluctuating convection velocity,” *J. Cryst. Growth*, vol. 220, no. 1–2, pp. 166–175, 2000.